Ocean Dynamics
DOI 10.1007/s10236-014-0745-2

Air–sea interactions during strong winter extratropical storms

Jill Nelson · Ruoying He · John C. Warner · John Bane

Received: 15 December 2013 / Accepted: 27 June 2014

Abstract A high-resolution, regional coupled atmosphere–ocean model is used to investigate strong air–sea interactions during a rapidly developing extratropical cyclone (ETC) off the east coast of the USA. In this two-way coupled system, surface momentum and heat fluxes derived from the Weather Research and Forecasting model and sea surface temperature (SST) from the Regional Ocean Modeling System are exchanged via the Model Coupling Toolkit. Comparisons are made between the modeled and observed wind velocity, sea level pressure, 10 m air temperature, and sea surface temperature time series, as well as a comparison between the model and one glider transect. Vertical profiles of modeled air temperature and winds in the marine atmospheric boundary layer and temperature variations in the upper ocean during a 3-day storm period are examined at various cross-shelf transects along the eastern seaboard. It is found that the air–sea interactions near the Gulf Stream are important for generating and sustaining the ETC. In particular, locally enhanced winds over a warm sea (relative to the land temperature) induce large surface heat fluxes which cool the upper ocean by up to 2 °C, mainly during the cold air outbreak period after the storm passage. Detailed heat budget analyses show the ocean-to-atmosphere heat flux dominates the upper ocean heat content variations. Results clearly show that dynamic air–sea interactions affecting momentum and buoyancy flux exchanges in ETCs need to be resolved accurately in a coupled atmosphere–ocean modeling framework.

Keywords Coupled modeling · Winter extratropical cyclones · East coast winter storms · Air/sea interaction · Gulf Stream · USA/east coast

Responsible Editor: John Wilkin

J. Nelson · R. He (✉)
Department of Marine, Earth, and Atmospheric Sciences, North Carolina State University, Raleigh, NC, USA
e-mail: rhe@ncsu.edu

J. C. Warner
U.S. Geological Survey, Coastal and Marine Geology Program, Woods Hole, MA, USA

J. Bane
Department of Marine Sciences, University of North Carolina, Chapel Hill, NC, USA

1 Introduction

Severe winter storms along and off the US east coast, commonly known as northeasters, are most frequent and intense in January (Colucci 1976; Zishka and Smith 1980; Hirsch et al. 2001). These fast-moving, extratropical cyclones (ETCs) are synoptic-scale low-pressure systems that often bring heavy precipitation, strong northeasterly winds, and bitterly cold temperatures to the mid-Atlantic and New England states and eastern Canada. The impacts of these storms can be especially devastating to coastal areas in these regions as a result of severe beach erosion due to storm-induced waves (DeGaetano 2008). Winter ETCs arguably cause more damage to the US east coast than tropical storms and hurricanes due to their high frequency between October and April and long duration (Hirsch et al. 2001). Widespread societal, economic, and environmental impacts are not uncommon (DeGaetano 2008). Several climatological studies indicate that the most favorable region for winter cyclone occurrence and intensification is parallel to the US–Canada east coast, stretching from North Carolina to Newfoundland (Colucci 1976; Sanders and Gyakum 1980; Zishka and Smith 1980). Particularly, strong cyclones (those with central pressure deepening rates of at least 24 hPa day^{-1} (Sanders and Gyakum 1980)) often develop near Cape Hatteras, North Carolina, in the surface convergence zone between a cold, dry Arctic air mass and the relatively warm marine air (>20 °C) overlying

Published online: 30 July 2014

the Gulf Stream and subtropical gyre waters of the Atlantic (Sanders and Gyakum 1980).

The Gulf Stream is a warm, swift western boundary current that meanders poleward along the southeastern US continental margin to Cape Hatteras where it then separates from the margin and travels northeastward and then eastward across the North Atlantic (Fig. 1). On average, the Gulf Stream is roughly 100 km wide and 1,000 m deep, and year-round surface temperatures typically exceed 24 °C. The ocean overlying the continental shelf north (south) of Cape Hatteras is known as the Middle (South) Atlantic Bight (hereafter called the MAB and SAB, respectively). Seaward of the Gulf Stream is the relatively warm, North Atlantic subtropical gyre, a basin-wide anticyclonic circulation system whose western portion close to the Stream is known as the Sargasso Sea. In winter, the cross-shelf sea surface temperature (SST) gradient is larger in the SAB than in the MAB because of the close proximity (<100 km) of the Gulf Stream to the coastline. Sharp changes in SST off the southeastern USA, where the cooler coastal water is adjacent to the warm Gulf Stream, induce energetic air–sea interactions. Of particular interest are the large ocean-to-atmosphere (atmosphere-to-ocean) heat (momentum) fluxes over the Gulf Stream, which can rapidly modify the marine atmospheric boundary layer (MABL) and influence storm development (Small et al. 2008).

Understanding the complex air–sea interactions that occur within the winter ETCs that regularly form or traverse over the eastern USA and intensify rapidly as they track across the western North Atlantic Ocean was the core objective of the Genesis of Atlantic Lows Experiment (GALE). The GALE field program was conducted from 15 January to 15 March 1986 (Dirks et al. 1988). This large, multi-investigator research program was designed to measure concurrent atmospheric and oceanic conditions at high spatial and temporal resolution so as to resolve modifications to the MABL and the upper ocean driven by the passage of an ETC. During GALE, Reddy and Raman (1994) observed the formation of a surface convergence zone (flow of near-surface air that causes an upward motion) as low-level winds accelerated toward the Gulf Stream and established a mesoscale circulation in the MABL. Both Bane and Osgood (1989) and Wayland and Raman (1994) reported near-surface turbulent

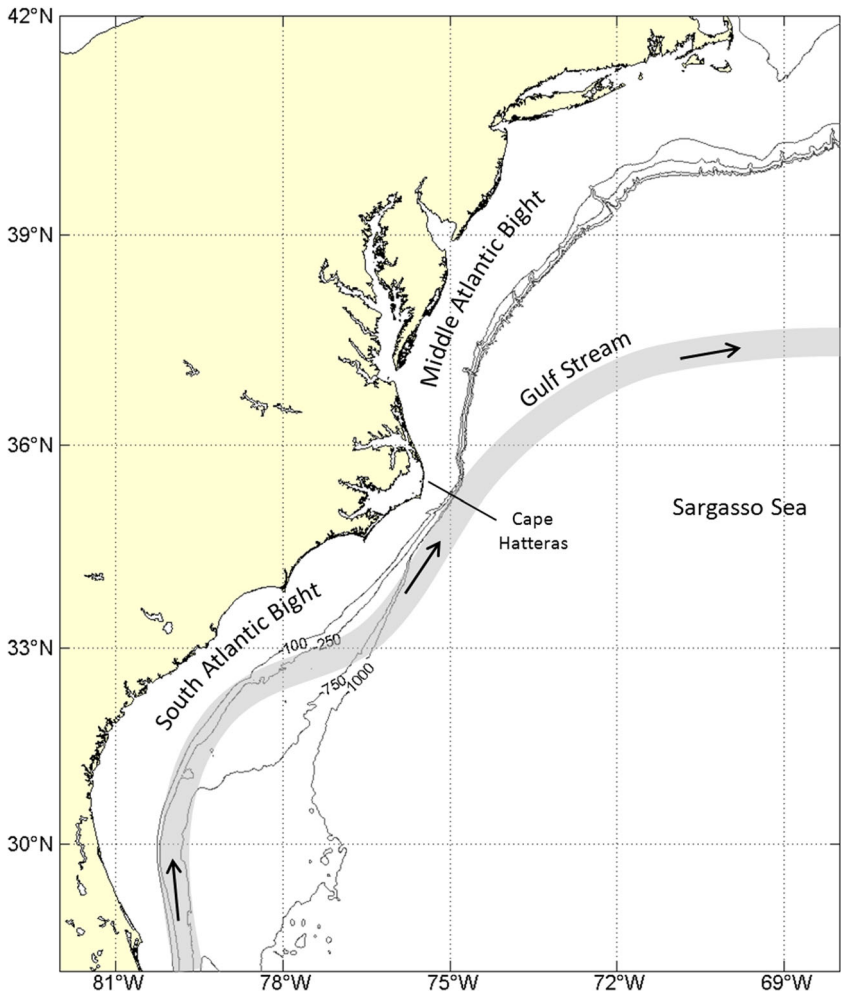

Fig. 1 Schematic showing the meandering pathway of the Gulf Stream relative to Cape Hatteras, the Middle Atlantic Bight (*MAB*), the South Atlantic Bight (*SAB*), and the Sargasso Sea. The isobaths are given in meters

atmospheric heat fluxes in excess of 1,000 W m^{-2} over the Gulf Stream due to large air–sea temperature and humidity differences during the 25–30 January 1986 storm and its accompanying cold air outbreak. Bane and Osgood (1989) also documented a 1–2 °C decrease in upper ocean temperature and a 35-m deepening of the ocean mixed layer over the 5-day storm period. The analysis by Xue et al. (1995) revealed that the decrease in heat content of the Gulf Stream's surface mixed layer was balanced by the large latent-plus-sensible heat flux from the ocean to the atmosphere during the cold air outbreak phase of this storm.

Recent advancements in regional, coupled atmosphere–ocean models have allowed more detailed analyses of air–sea exchanges and feedbacks during ETCs. In the present study, we utilize the newly developed Coupled-Ocean-Atmosphere-Wave-Sediment-Transport (COAWST) modeling system to assess strong air–sea interactions during an intense east coast winter ETC. This case study is of a storm that formed offshore near Cape Hatteras and rapidly developed into a powerful cyclone on 23 January 2005. A detailed description of the three-dimensional, coupled atmosphere–ocean model and discussions on model configuration are given in Section 2. A synoptic description of the prevailing weather pattern in January 2005 is given in Section 3. Section 4 presents model validations against in situ observations from marine meteorological buoy and ocean glider data. Discussions on the coupled model results, including the feedbacks between the MABL and the upper ocean and the oceanic heat budget for this storm, are given in Section 5. Final discussions and conclusions are in Section 6.

2 Model and data

2.1 Coupled model description

The COAWST modeling system was developed to investigate storm impacts on coastal ocean environments (Warner et al. 2010). The fully coupled system consists of four model components: the Regional Ocean Modeling System (ROMS) (Shchepetkin and McWilliams 2005), the Weather Research and Forecasting (WRF) model (Skamarock et al. 2008), the Simulating Waves Nearshore (SWAN) model (Booij et al. 1999), and the Community Sediment Transport Model (CSTM) (Warner et al. 2008). The Model Coupling Toolkit (MCT) facilitates the exchange of key atmospheric and oceanic fields between models (Larson et al. 2005). The COAWST configuration for this study is comprised of WRF and ROMS coupling only. We note that Olabarrieta et al. (2012) used WRF, ROMS, and SWAN coupling to investigate the atmosphere–ocean–wave interactions in November 2009 during the merger of Hurricane Ida with a nor'easter storm.

Specifically, we apply WRF ARW Version 3.1 in this study. WRF ARW (Advanced Research WRF dynamical core, http://www.wrf-model.org) integrates the fully compressible, non-hydrostatic governing equations on a terrain-following vertical coordinate system. It offers sophisticated physics parameterization schemes for handling surface radiation fluxes, boundary layer processes, and precipitation processes. Longwave and shortwave radiation physics are computed by the Rapid Radiative Transfer Model (RRTM) and the Goddard scheme, respectively. The Monin-Obukhov atmospheric surface layer model and the Noah land surface model are used in conjunction with the Mellor-Yamada-Janjic (MYJ) 1.5-order prognostic turbulent kinetic energy (TKE) planetary boundary layer (PBL) scheme. The atmospheric and land surface layer models calculate exchange coefficients and surface fluxes off the land or ocean surface and pass them to the MYJ PBL model every time step. The WRF Single-Moment (WSM) six-class moisture microphysics scheme represents grid-scale precipitation processes (vapor, cloud, rain, snow, ice, and graupel), and the Kain-Fritsch cumulus scheme represents subgrid scale convection and cloud detrainment.

The ROMS ocean circulation model is a free-surface, hydrostatic, primitive equation model used extensively for estuarine, coastal, and basin-scale research applications (http://www.myroms.org). The ROMS coordinate system is formulated on a horizontal curvilinear Arakawa C-grid with stretched, terrain-following vertical levels. ROMS includes various accurate, high-order numerical schemes for subgrid scale advection and diffusion. We use the Mellor-Yamada (1982) level-2.5 closure scheme to compute vertical turbulent mixing, as well as the quadratic drag formulation for the bottom friction specification.

Fields exchanged in the two-way coupled WRF/ROMS system are surface momentum flux (τ), net heat flux, and sea surface temperature (Fig. 2). The time steps for WRF and ROMS are 60 and 300 s, respectively. During the simulation, surface momentum and heat fluxes generated by WRF and SST by ROMS are exchanged on each coupling time interval, which is every 600 s.

2.2 Datasets

Initial and lateral boundary conditions for WRF are obtained from NCEP North American Regional Reanalysis (NARR).

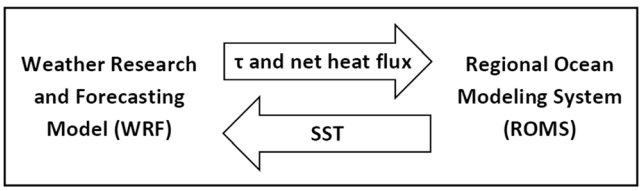

Fig. 2 A diagram showing the fields exchanged in the two-way coupled WRF/ROMS model simulation

NARR reanalysis data are available for North America since January 1979 at three-hourly intervals with 1/3° (~35 km) spatial resolution.

Initial and lateral boundary conditions for ROMS are acquired from the Hybrid Coordinate Ocean Model (HYCOM) Navy Coupled Ocean Data Assimilation (NCODA) simulation. The global HYCOM NCODA output is available daily at 1/12° (~10 km) spatial resolution since November 2003. Open boundary conditions were applied at the southern and eastern boundaries (Fig. 3) to tracers and baroclinic velocity following the method of Marchesiello et al. (2001). Free-surface and depth-averaged velocity boundary conditions were specified using the method of Flather (1976) with the external values defined by HYCOM. Tides and rivers are excluded from this ocean model setup since our focus here is on wintertime, synoptic-scale, air–sea interactions.

2.3 Model setup

We ran the model simulation from 13 to 31 January 2005, during which time a total of five extratropical cyclones impacted the eastern USA. The COAWST domain encompasses central and eastern North America, the Gulf of Mexico, and the western North Atlantic Ocean (Fig. 3). The WRF grid is 225×236 in the east–west and north–south directions, respectively, with 15 km horizontal resolution and 48 vertical levels. The ROMS grid is 774×832 with 5 km horizontal resolution and 18 vertical levels. Both WRF and ROMS are run over the entire COAWST model domain and diagnostics are output every 3 h. The Spherical Coordinate Remapping and Interpolation Package (SCRIP; Jones 1998) program is used to create flux-conserving interpolation weights between the different model grids. By this means, surface momentum and heat fluxes from WRF are interpolated to the ROMS model grid, and SST from ROMS is interpolated to the WRF model grid for field exchanges. The final COAWST grid uses a Mercator projection.

3 Synoptic description

The observational time series (Fig. 4) from National Data Buoy Center (NDBC) buoy 44009 located 30 km off the Delaware coast (Fig. 3) clearly reveals a calm weather pattern from 1 to 12 January 2005. This is followed by a period of enhanced storm activity from 13 to 31 January 2005. NDBC buoys 41004 (located 75 km east of Charleston, South Carolina) and 44009 (located 50 km southeast of Cape May, New Jersey) reported similar trends due to the large alongshore span of east coast ETCs (see Fig. 5). During the first half of January, mild predominantly southerly winds prevailed with 10 m air temperatures about the same as the ocean surface

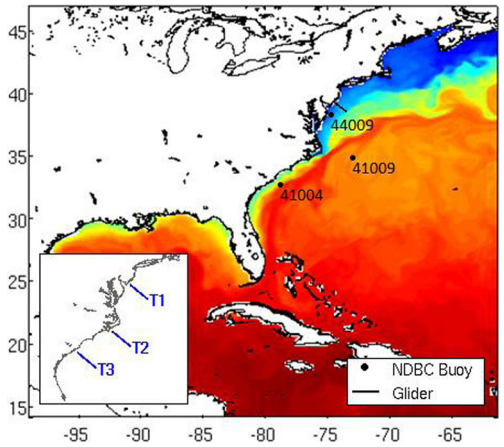

Fig. 3 The COAWST model domain encompasses central and eastern North America, the Gulf of Mexico, and the western Atlantic Ocean. Both WRF and ROMS grids are run over the entire COAWST domain. *Color shading* represents the high-resolution SST field simulated by COAWST. Also shown are the locations of the three NDBC buoys (44009, 41001, and 41004), the Endurance Line glider transect, and the cross-shelf transects (*blue*; T1, T2, and T3) along which the air–sea feedbacks are examined

temperatures and low (around zero) sensible and latent heat fluxes (see Fairall et al. (1996)) for a description of the heat flux equations). In contrast, the second half of the month (13–31 January) was characterized by five fast-moving ETCs, sharp drops in air temperature (up to 20 °C) and ocean temperature (up to 5 °C), and moderate combined sensible

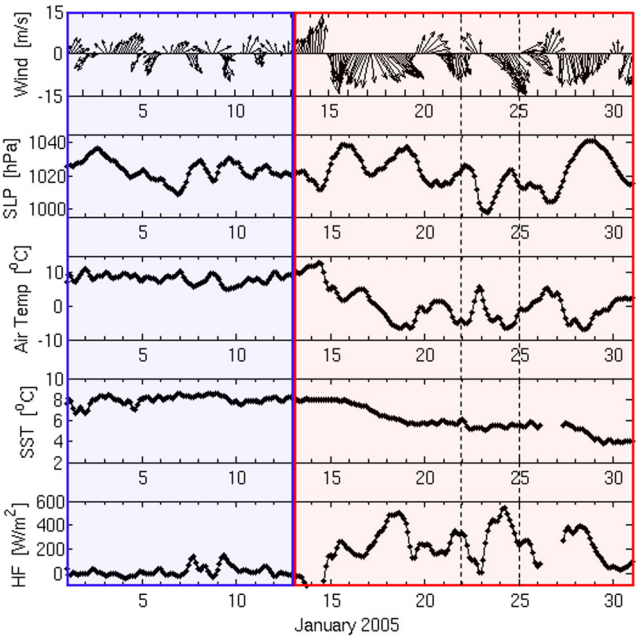

Fig. 4 Time series of the 10-m wind, SLP, 10-m air temperature, SST, and total sensible, and latent heat flux (*HF*) observed at buoy 44009 in January 2005. A calm weather period (*blue*) is followed by a period of enhanced storm activity in the second half of the month (*red*). The effects of the strong 22 to 23 January ETC are indicated between the *black dashed lines*

and latent heat fluxes from the cool MAB shelf waters (both positive, up to 600 W m^{-2} total flux). At buoy 41004, a total ocean-to-atmosphere heat flux of approximately 1,050 W m^{-2} was measured out of the warmer Gulf Stream, in good agreement with the maximum fluxes reported by Wayland and Raman (1994) and Bane and Osgood (1989) during the GALE program.

The dynamical focus of the present analysis is on the powerful ETC that impacted the study area from 22 to 25 January 2005. On 22 January 21Z, a 1,002-hPa low-pressure center formed over the coastal area to the north of Cape Hatteras (Fig. 5). This region of low pressure intensified into an ETC with upper-level support from a 500-hPa trough over the eastern USA (not shown). Over the first 12 h, the ETC's central pressure dropped rapidly by 16 hPa as the cyclone tracked northeastward, and a cold front oriented northeast to southwest swept over the MAB and SAB. The cyclone continued deepening to at least 980 hPa after 24 h. Enhanced northwesterly winds persisted over the MAB for 2 days after the cold front moved through, due to the counterclockwise circulation around the low-pressure center as the ETC moved out of the study region. The near-freezing air temperatures and high wind speeds after the storm's passage (see between the dashed lines on Fig. 4) provided strong atmospheric forcing to the underlying ocean.

4 Coupled model performance

The performance of our coupled model simulation is gauged against the hourly time series of surface winds, sea level pressure (SLP), air temperature, and SST measured by NDBC buoys 44009, 41004, and 41001, as well as ocean temperature measured along the Rutgers University Endurance Line glider transect (see locations in Fig. 3) across the northern MAB continental shelf. NDBC buoy measurements are located in three distinct ocean regimes: the cool shelf water in the MAB (buoy 44009), the seaward side of the Gulf Stream offshore of Cape Hatteras (buoy 41001), and the warm mid-shelf water in the SAB (buoy 41004). Buoy data are 36-h low-pass filtered and subsampled every 3 h to be concurrent with model output over the time period 13–31 January 2005. In situ observations are directly compared to the corresponding value at the closest model grid point or model transect. Each model data wind time series comparison is quantified by a vector correlation coefficient (r), vector orientation difference (Θ, in degree true north), and vector regression coefficient (Reg) (e.g., Kundu (1976)). Air temperature, SLP, and SST comparisons are quantified by their correlation coefficient (r) and root mean square error (RMS error).

The wind time series comparison (Fig. 6) shows excellent correspondence between in situ winds and winds from the coupled simulation (correlation coefficients greater than 0.84).

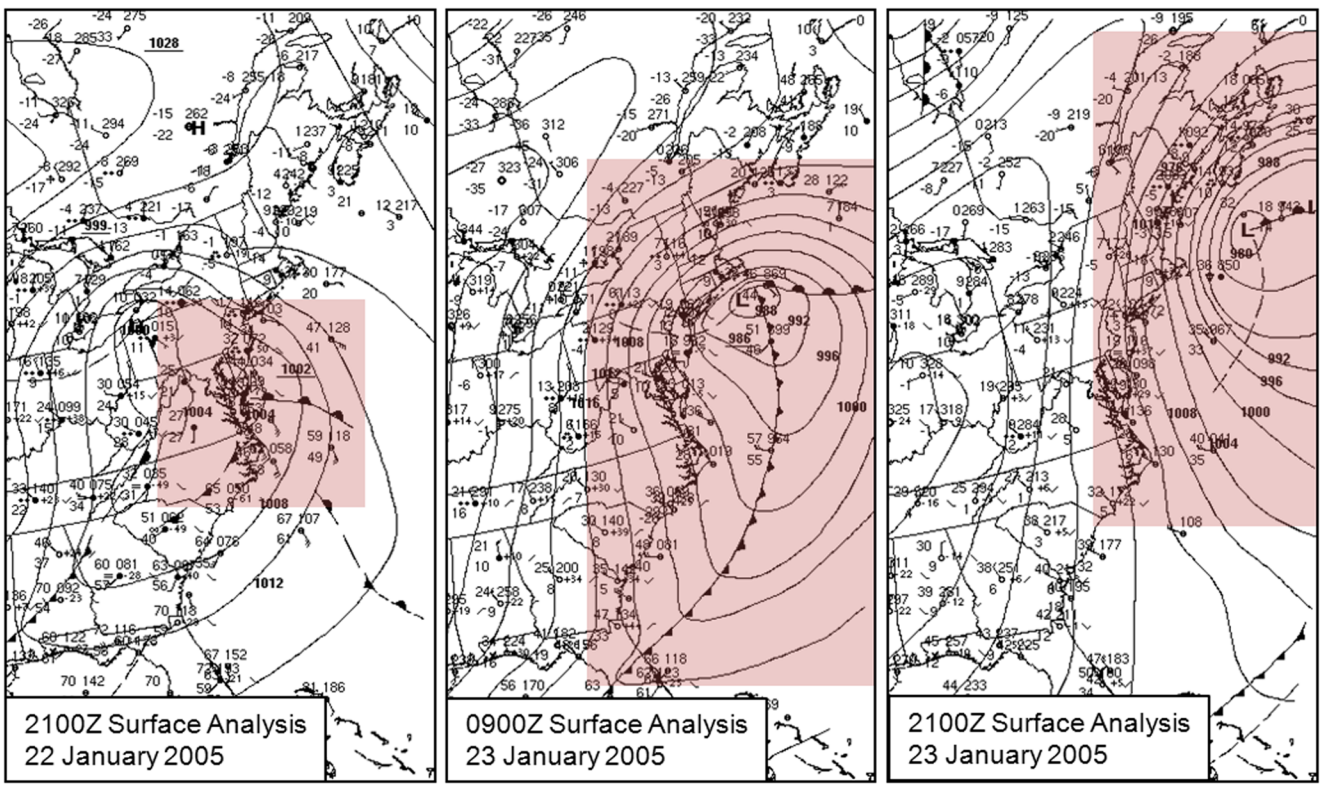

Fig. 5 Sequence of surface analysis charts depicting the progression of the strong ETC that impacted the study area in late January 2005

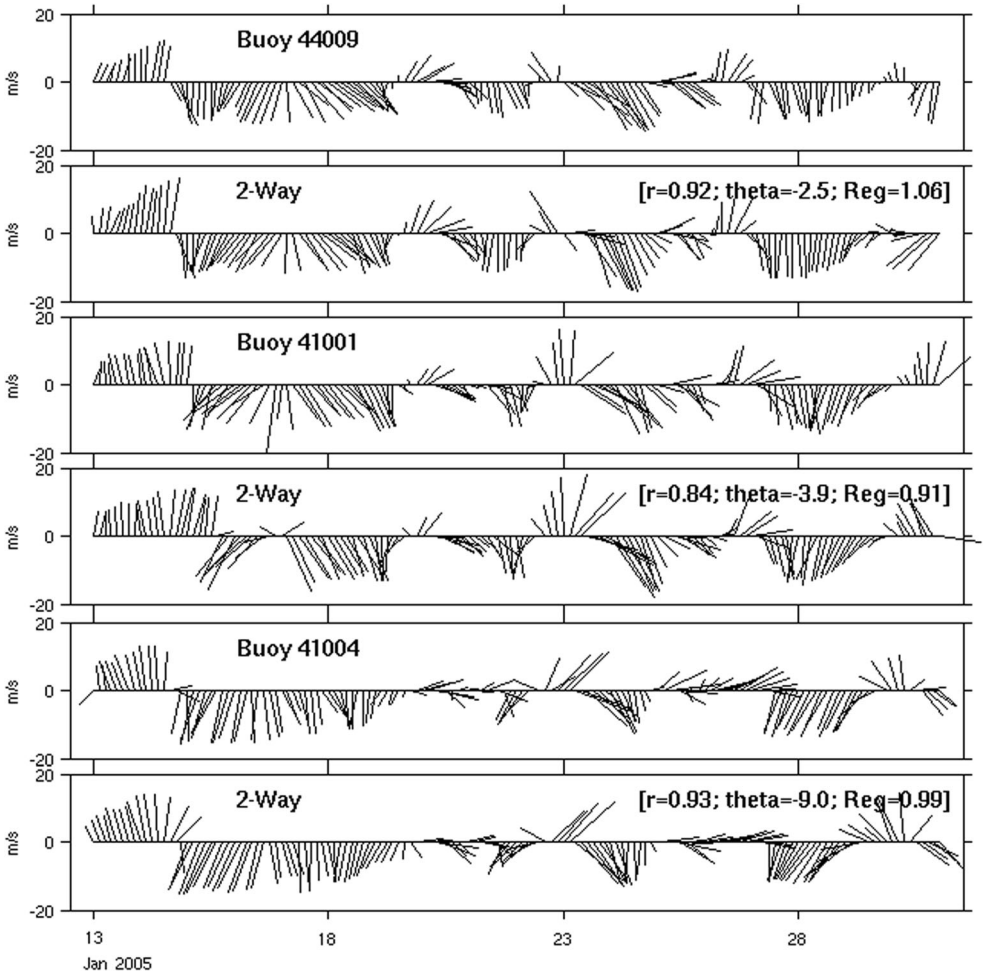

Fig. 6 Comparison between buoy-observed and simulated 10-m wind time series. Also shown are the complex correlation (r, Θ) and vector regression coefficient (*Reg*)

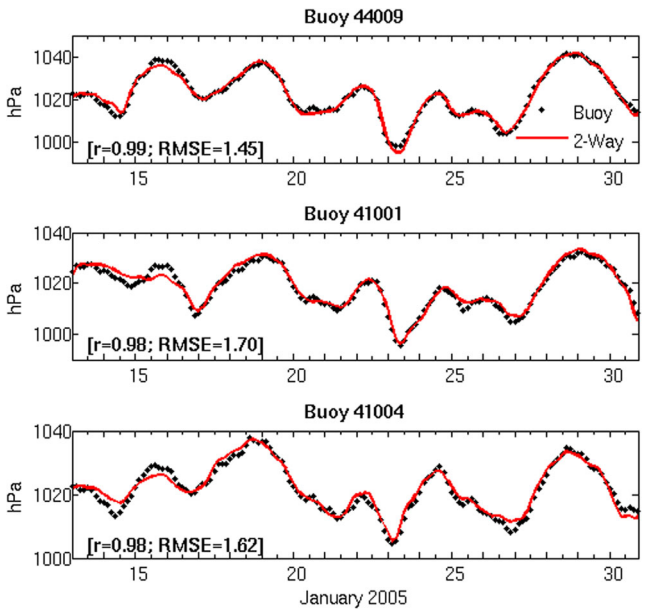

Fig. 7 Comparison between buoy-observed (*black*) and simulated (*red*) sea level pressure time series. Also shown are the correlation coefficients (r) and RMS error

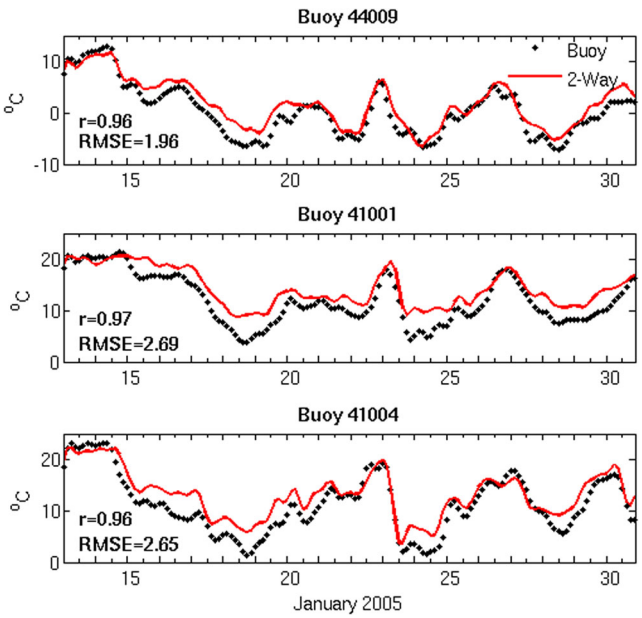

Fig. 8 Comparison between buoy-observed (*black*) and simulated (*red*) 10-m air temperature time series. Also shown are the correlation coefficients (r) and RMS error

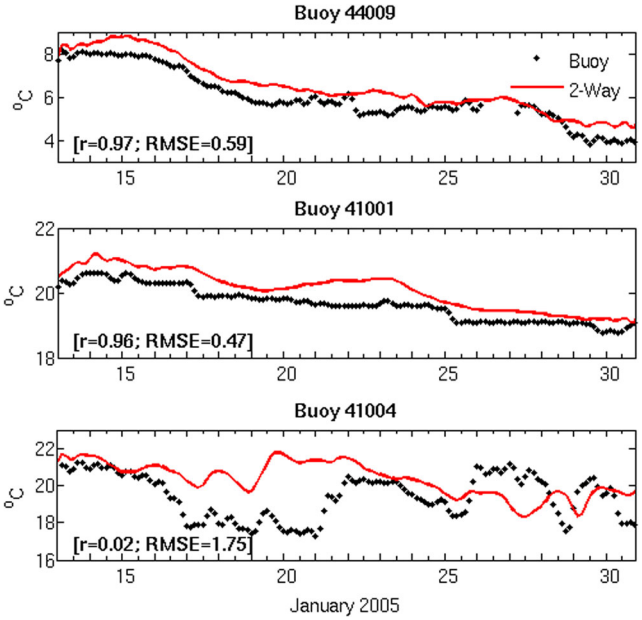

Fig. 9 Comparison between buoy-observed (*black*) and simulated (*red*) sea surface temperature time series. Also shown are the correlation coefficients (*r*) and RMS error

In particular, the coupled air–sea model successfully captures the high wind speeds (regressions ranging from 0.99 to 1.06) and the sharp changes in wind direction (mean offsets only about 5° in the clockwise direction) with each passing storm.

Modeled SLP also matches well with buoy-measured SLP (Fig. 7). The correlation coefficients are greater than 0.98 with mean offsets of about 1.5 hPa. Similarly favorable agreement is found in the 10-m air temperature prediction. The coupled simulation reproduces the temporal variability in the near-surface air temperature well, with correlation coefficients greater than 0.96 (Fig. 8). We note that the model overestimates (by up to roughly 2.7 °C) air temperature during ETCs. We speculate that the model contains a small "warm bias" as it does not take into account cooling from enhanced evaporation due to storm-induced wave breaking.

SST comparisons (Fig. 9) are reasonable as well, except at buoy 41004. The differences are due to a number of factors, including the spatial offsets between the buoy point measurement and the corresponding point on the ocean model's 5-km footprint, and the difference between the bulk ocean temperature measured 1 m below the surface by the buoy and temperature of the uppermost vertical layer simulated by the model. For 41004 in particular, the small lateral movements of the Gulf Stream on the SAB shelf from 16 to 22 January are not well captured by the ocean model, and for the remainder of January, the modeled temperatures lag behind the observed surface temperature, resulting in a low correlation at this station. Nevertheless, temperature time series are highly correlated (>0.96) with less than 0.6 °C bias at the other two buoy stations (44009 and 41001).

The shelf temperature comparison between the glider observations and the coupled simulation on 14 January 2005 is very good (Fig. 10). The ROMS ocean model accurately reproduces the vertically well-mixed shelf waters, the horizontal temperature gradient (increasing from 7 to 9 °C in the offshore direction), and most of the small-scale horizontal temperature structures. Slight discrepancies are apparent between the model and observations in the cool waters nearshore and the warm waters 80 to 100 km offshore.

Based on the degree of comparison between model and data, it seems reasonable that our dynamical analysis described below is couched in a realistic air–sea environment.

5 Coupled model analysis

5.1 Atmosphere–ocean feedbacks

To illustrate the air–sea interactions during the passage of this intense winter ETC over the western North Atlantic, we examine vertical profiles of variables within the upper ocean and the lower atmosphere across three cross-shelf transects. Transect T1 spans the central MAB shelf and shelf break, T2

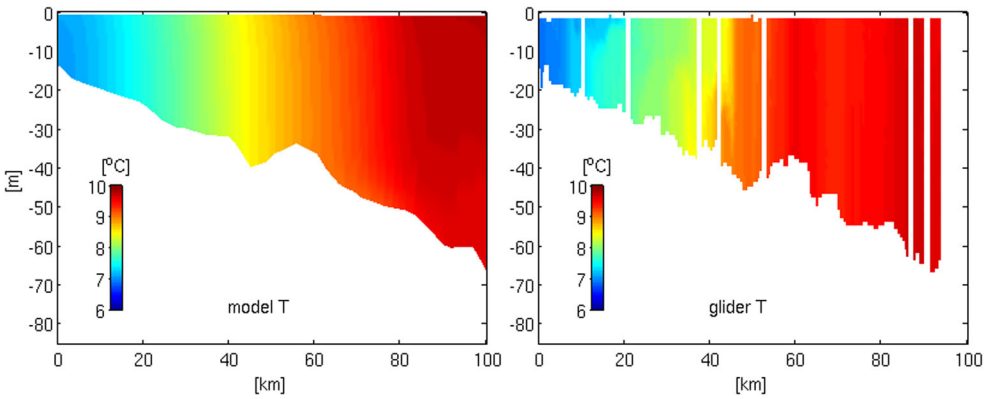

Fig. 10 Comparison between glider-observed (*right panel*) and simulated (*left panel*) cross-shelf ocean temperature structure along the Endurance Line (see location in Fig. 7) on 14 January 2005

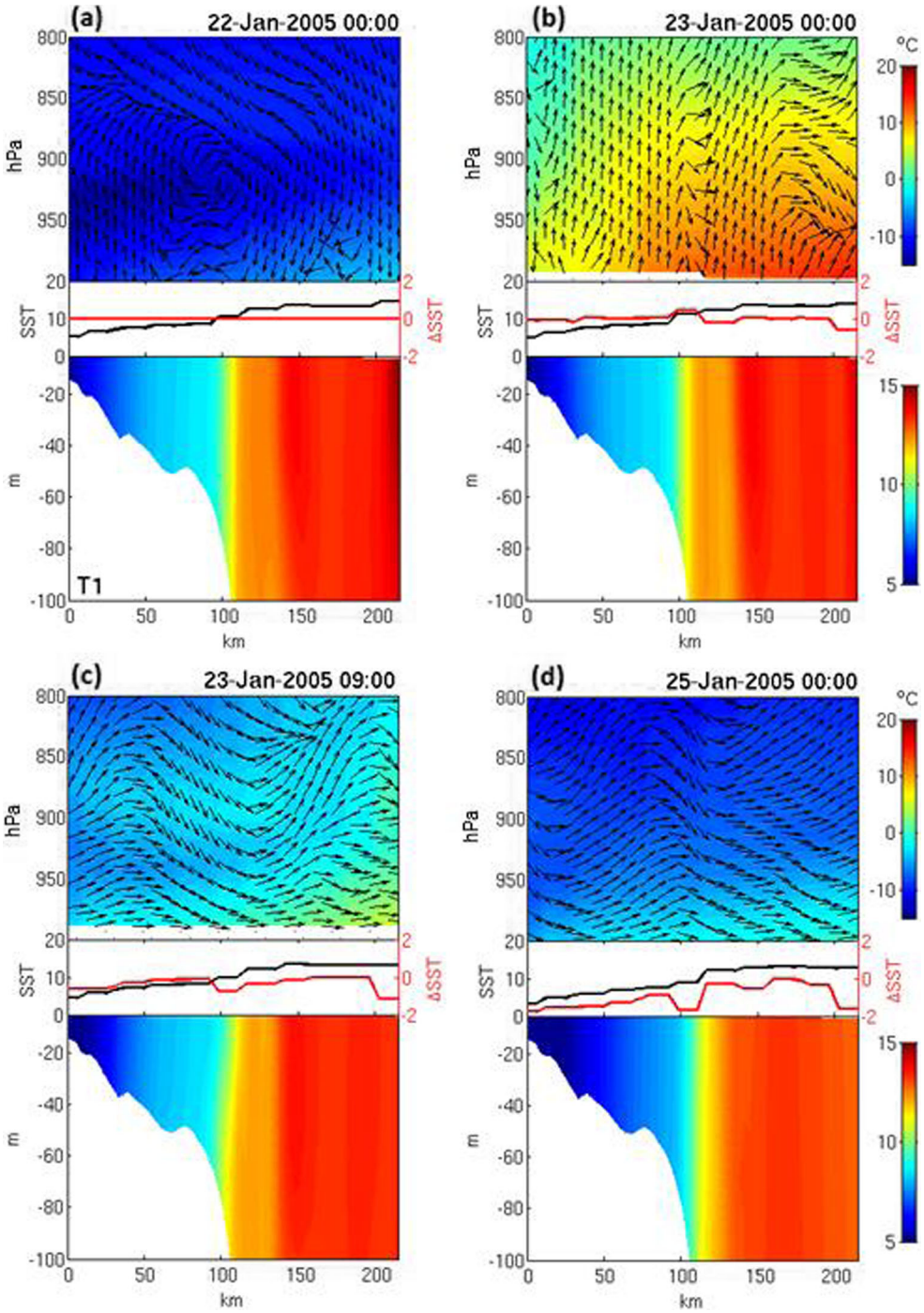

Fig. 11 **a**–**d** Vertical profiles of the air temperature and normalized wind field in the MABL and the underlying ocean temperature along transect T1. Also shown are the corresponding along-transect SST profiles (*black*) and the temperature change relative to the pre-storm SST at 22 January 00Z (*red*). Current direction beyond 100 km offshore is into the page

spans the northern SAB shelf and the Gulf Stream about 50 km south of Cape Hatteras, and T3 spans the central SAB shelf and the Gulf Stream perpendicular to the South Carolina shoreline just south of Cape Romaine (see blue lines in Fig. 3). Each transect is 250-km long, and they are spaced roughly 300 km apart along the eastern seaboard. For brevity, we selected to show profiles associated with the pre-storm conditions (22 January 00Z), ETC formation (23 January 00Z), the onset of the cold air outbreak following the frontal passage (23 January 09Z), and the end of the cold air outbreak (25 January 00Z). An animation showing all of the vertical profiles at three-hourly intervals from 22 to 25 January 2005 can be viewed online at http://omglnx7.meas.ncsu.edu/jsnelson/profile_anim/atm2ocn.htm. Along each transect, profiles of the air temperature and normalized vertical wind field of the MABL and the water temperature in the upper 100 m of the underlying ocean are shown in Figs. 11, 12, and 13.

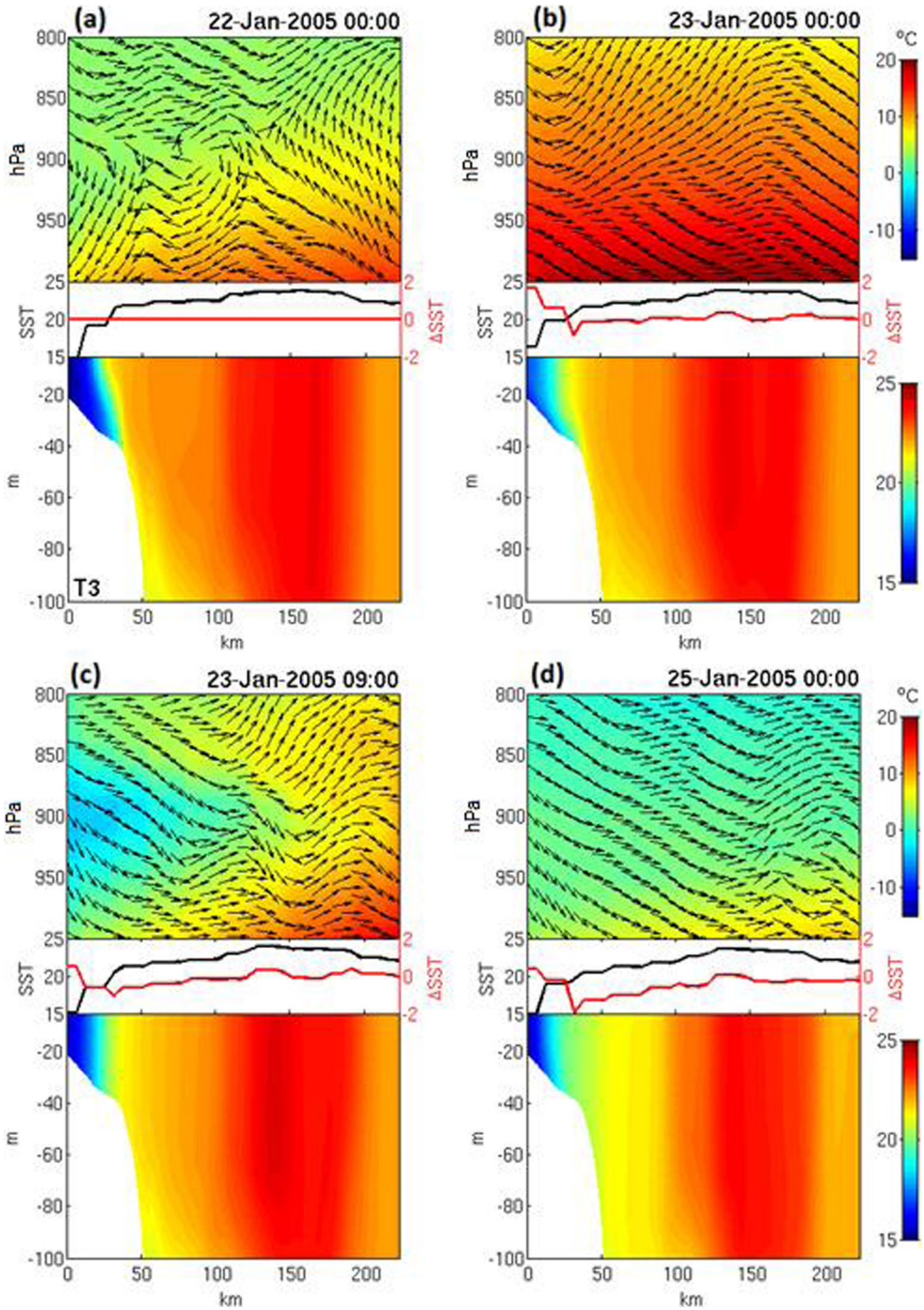

Fig. 12 **a**–**d** Vertical profiles of the air temperature and normalized wind field in the MABL and the underlying ocean temperature along transect T2. Also shown are the corresponding along-transect SST profiles (*black*) and the temperature change relative to the pre-storm SST at 22 January 00Z (*red*). Current direction beyond 50 km offshore is into the page

The corresponding along-transect SST is highlighted and overlaid with the magnitude of the temperature change (ΔSST) between the instantaneous SST profile and the pre-storm SST profile (defined as the SST on 22 January 00Z). In Fig. 14, we also present a sequence of maps showing the evolution of the atmospheric forcing conditions (simulated 10 m air temperature, SLP, and 10 m horizontal wind vectors) from 1 day prior to the storm's formation to the end of the cold air outbreak (22 to 25 January 00Z).

On 22 January 00Z, northerly winds prevail over the western Atlantic Ocean due to the clockwise circulation around a synoptic high pressure system located over the northeastern USA. Along the northernmost transect (T1), the water column is well-mixed with water temperatures of ~8 °C near the coast increasing to ~14 °C beyond the MAB shelf break (Fig. 11a). The air temperatures throughout the MABL are below freezing along T1 with slightly warmer near-surface air temperatures over the shelf break waters. Off Cape Hatteras, warm

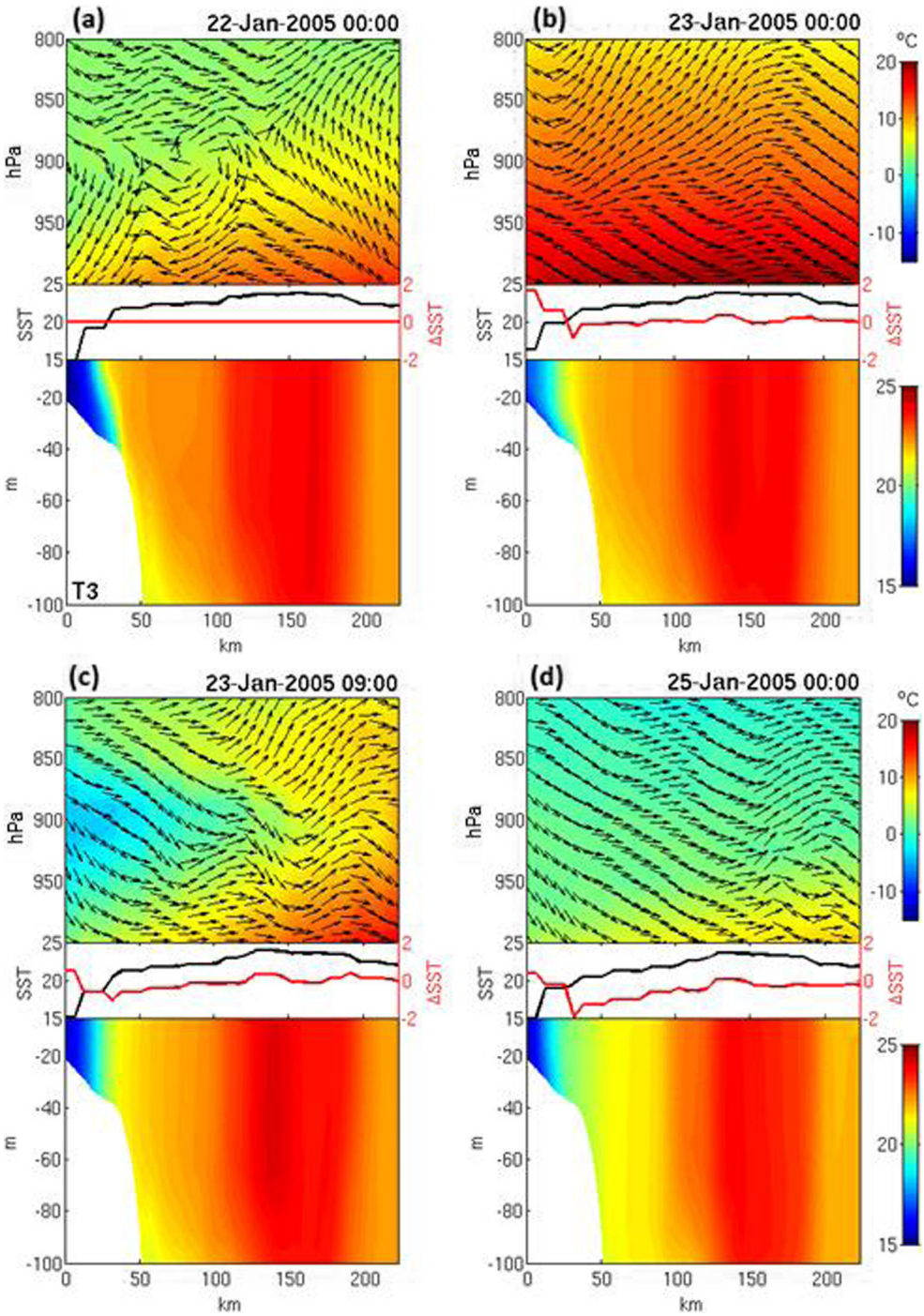

Fig. 13 **a**–**d** Vertical profiles of the air temperature and normalized wind field in the MABL and the underlying ocean temperature along transect T3. Also shown are the corresponding along-transect SST profiles (*black*) and the temperature change relative to the pre-storm SST at 22 January 00Z (*red*). Current direction beyond 50 km offshore is into the page

(23 °C) Gulf Stream waters are present 40 km from the shoreward end of T2, separating slightly cooler waters (both ~20 °C) over the well-mixed SAB shelf and Sargasso Sea (Fig. 12a). The Gulf Stream is farther offshore and slightly warmer at T3, the southernmost transect, than at T2 (Fig. 13a). Pre-storm, surface air temperatures are ~10 °C warmer over the Gulf Stream along T2 and T3 than at the coast as shallow mesoscale atmospheric circulations effectively warm the MABL to 900 hPa.

Over the next 24 h, the high pressure system moves away from the study region and the incipient ETC forms off Cape Hatteras. By 23 January 00Z, the low-pressure center of the ETC is positioned over T1, while T2 and T3 are in the ETC's warm sector and the prevailing south-southwesterly flow over the Atlantic Ocean begins accelerating toward the ETC center. At this time, the inflow of warm air from the south converges over the Gulf Stream and destabilizes the atmosphere, generating upward motions and warming the MABL by 10–15 °C

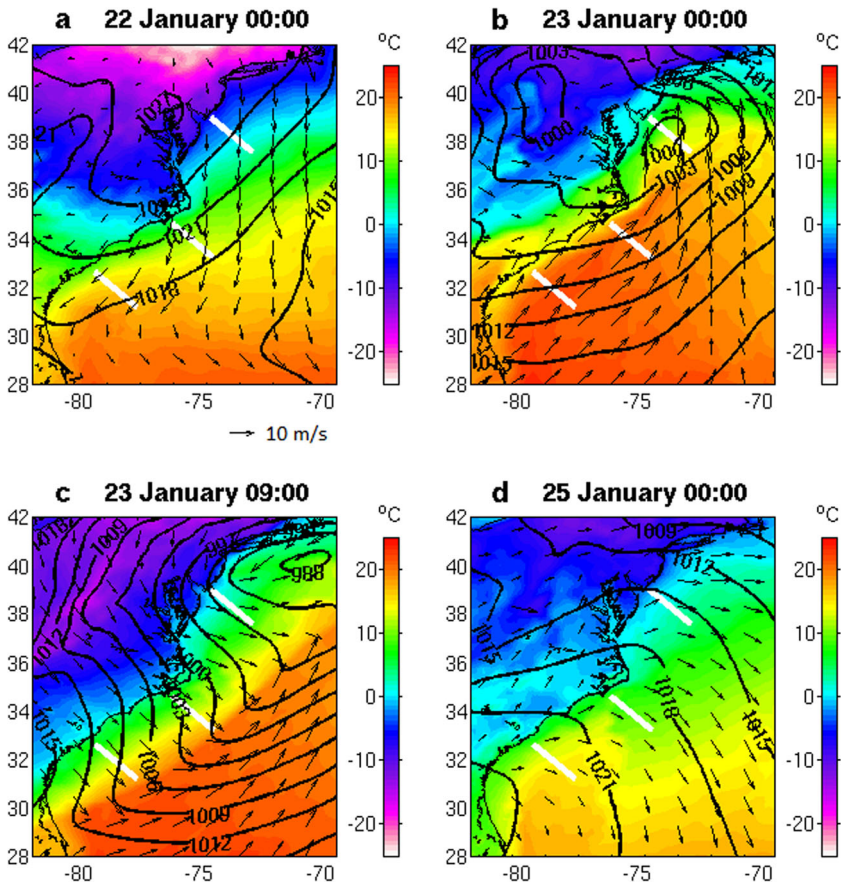

Fig. 14 **a**–**d** Simulated 2 m air temperature (*shaded*), sea level pressure (*contours*; 3 hPa interval), and 10-m horizontal wind vectors depicting the evolution of the atmospheric forcing conditions from 1 day prior to the storm's formation to the end of the cold air outbreak (22 to 25 January 00Z). The transect locations (*white*; T1 to the *north*, T2 in the *middle*, and T3 to the *south*) are also given

(Figs. 11, 12, and 13b). The energetic upward winds and the MABL heating sustain the intensifying cyclone over the next several hours. The upper ocean temperature response is small (<1 °C ocean temperature decrease at each location) during this early stage of this ETC development.

The cold air outbreak over the ocean begins at 23 January 09Z when a cold, dry air mass sweeps offshore behind the cold front and lasts until 25 January 00Z. Most of the ocean cooling occurs during these 2 days (Figs. 11, 12, and 13). Storm-enhanced winds and prolonged surface-ocean contact with cold, dry air drive greater ocean-to-atmosphere sensible and latent heat fluxes. These large heat fluxes out of the ocean cause the MAB shelf waters and the Gulf Stream to cool up to 2 °C. The MABL quickly reverts back to pre-storm conditions after the cold air outbreak, as a ridge of high pressure builds into the eastern USA. The ocean temperatures are slower to recover, although the warm northward-flowing Gulf Stream waters will eventually replenish the heat lost across T2 and T3.

5.2 Oceanic heat budget

To identify the processes resulting in the roughly 2 °C temperature drop that occurs within the upper 100 m of the ocean during the ETC passage, we quantify the oceanic heat budget along transects T1, T2, and T3. Temperature changes in the ocean are governed by the thermodynamic equation:

$$\frac{\partial T}{\partial t}+\left[u\frac{\partial T}{\partial x}+v\frac{\partial T}{\partial y}+\frac{\partial T}{\partial z}\right]=\frac{\partial}{\partial z}\left(K\frac{\partial T}{\partial z}\right)+\frac{\partial}{\partial x}\left(A\frac{\partial T}{\partial x}\right)+\frac{\partial}{\partial y}\left(A\frac{\partial T}{\partial y}\right). \quad (1)$$

where u, v, and w are the cross-shore (x-direction), alongshore (y-direction), and vertical (z-direction) velocity components, T is ocean temperature (°C), t is time, K is the vertical eddy thermal diffusivity, and A is the horizontal eddy viscosity. The rate of temperature change $\left(\frac{\partial T}{\partial t}\right)$ is directly influenced by horizontal and vertical advection (bracketed terms on the left-hand side) and horizontal and vertical diffusion (terms on the right-hand side). We note that the horizontal diffusion term is negligible (not shown), but vertical diffusion can be quite large during a winter storm (Xue et al. 1995). As described in the next paragraph, the radiative energy fluxes at the air–sea interface are cast as boundary conditions at the sea surface.

We diagnose the heat budget along three cross-shelf sections where the lateral boundaries are defined as the onshore

and offshore ends of each transect, the top boundary is the sea surface, and the bottom boundary is set to a depth of 100 m. Depth-integrating Eq. 1 over the upper 100 m of the water column along each transect for the 3-day storm period (22–25 January 2005), in conjunction with the boundary condition of ocean temperature, yields the following heat balance equation:

$$\Delta H = H_{\mathrm{adv}} + H_{\mathrm{flux}} \tag{2}$$

where $\Delta H = \rho C_p \int_{-100}^{\eta} \frac{\partial T}{\partial t} dz$ is the local rate of change in heat content of the section resulting from the vertical and horizontal heat advection through the water column $H_{\mathrm{adv}} = \rho C_p \int_{-100}^{\eta} \left(-u\frac{\partial T}{\partial x} - v\frac{\partial T}{\partial y} - w\frac{\partial T}{\partial z}\right) dz$, and the vertical and horizontal heat diffusion $H_{\mathrm{flux}} = Q - \left(K\frac{\partial T}{\partial z}\right)_{z\ =\ -100\ \mathrm{m}}$, where Q is the net surface heat flux (the sum of sensible heat, latent heat, shortwave radiation, and longwave radiation), $\left(K\frac{\partial T}{\partial z}\right)_{z\ =\ -100\ \mathrm{m}}$ is the heat diffusion at 100 m, and ρ and C_p are seawater density (1,025 kg m^{-3}) and specific heat (3,990 J kg^{-1} K^{-1}), respectively. The vertical heat flux across the bottom of the section is very small (not shown), being only about −5 W m^{-2} on average, and so it is ignored in the following discussion. Negative (positive) results indicate ocean cooling (warming) (Fig. 15).

Along all three transects, common features in the oceanic heat budget include (1) the net surface heat fluxes (H_{flux}) are all negative, indicating that the ocean is losing heat to the atmosphere over the 3-day storm period; (2) large, rapid cooling occurs on 23 January, followed by a steady warming trend; and (3) the high-frequency variations in oceanic heat content (left column of Fig. 15) are determined by ocean advection.

The temporal mean (3-day average) heat budget provides an interesting insight on regional contrast. At T1, both H_{flux} and H_{adv} contribute to the ocean cooling, roughly at 80 and 20 % of ΔH (−600 W m^{-2}), respectively (Fig. 15a). A major portion of transect T1 is located on the MAB shelf (<100 m water depths), where significant water temperature decreases and moderate sensible and latent heat fluxes were observed by buoy 44009 (between the dashed lines in Fig. 4). Thus, shallow water temperature changes at this location resulted primarily from the heat flux into the atmosphere during ETC passage.

Both transects T2 and T3 span the Gulf Stream and present a different heat balance. Due to the persistent transport of

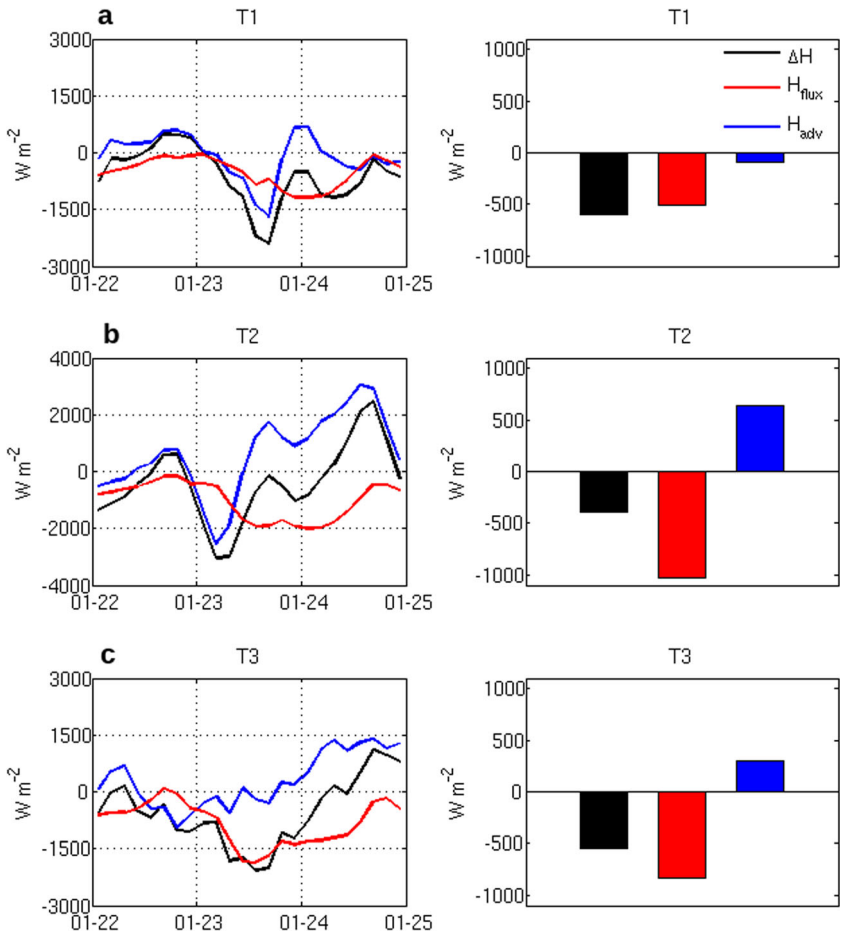

Fig. 15 **a**–**c** Upper ocean heat budget diagnosis at three sections along the eastern seaboard during the 3-day storm period (22–25 January). The *left column* shows the time series of the local rate of heat change ΔH, net surface heat diffusion H_{flux}, and net heat advection H_{adv} averaged over each cross-shelf transect, and the *right column* shows a bar plot of their corresponding temporal (3-day) mean values

warmer waters from the south, the warming effect of ocean advection and the cooling effect of surface heat flux counteract each other, resulting in a weaker cooling tendency compared to T1. This is especially true at T2 off Cape Hatteras, where the ocean advection associated with the Gulf Stream is the strongest. Nevertheless, the very large ocean-to-atmosphere heat flux during this ETC remains the dominant process for the upper ocean temperature budget. For all three transects, the net cooling tendency due to heat fluxes is two to four times larger than the net warming tendency due to heat advection.

6 Discussion and conclusion

We have utilized the COAWST modeling system to couple the WRF atmosphere model to the ROMS ocean model. The momentum flux, heat flux, and SST fields are exchanged between WRF and ROMS in this two-way coupled configuration. In general, the coupled simulation accurately reproduced the observed atmospheric and oceanic conditions during the late January 2005 ETC sequence comprising five total storms. We selected for the case study a winter extratropical cyclone that formed near Cape Hatteras and intensified rapidly as it tracked across the northwestern Atlantic Ocean. Atmosphere–ocean fluxes and feedbacks were examined in detail for this particular storm and attendant cold air outbreak (22 to 25 January), though major fluxes only occurred after the storm's passage. We show that surface wind convergence over the Gulf Stream (along the cold front) induces energetic mesoscale circulations that rapidly warm the MABL yet cause little to no upper ocean response during the ETC's early development stage. Near-freezing air temperatures and high wind speeds behind the cold front provide strong atmospheric forcing to the underlying ocean over the next couple of days. The large ocean-to-atmosphere surface heat fluxes, particularly during the cold air outbreak, cause the MAB shelf waters and the Gulf Stream to cool up to 2 °C, consistent with the magnitude of the upper ocean temperature decrease observed by Bane and Osgood (1989) and Xue et al. (1995). From the heat budget perspective, both oceanic heat loss and, to a smaller degree, oceanic advection contribute to the cooling on the shallow MAB shelf. In contrast, near the Gulf Stream (transects T2 and T3), the ocean cooling effect due to surface heat fluxes is offset somewhat by the smaller warming effect of Gulf Stream advection. For all locations, net cooling is observed and is dominated by the large surface heat fluxes out of the ocean.

In addition to the two-way coupled air–sea simulation presented above, two other model sensitivity experiments were performed to demonstrate the importance of air–sea coupling during winter extratropical cyclones, including (1) *uncoupled run*, WRF-only simulation with a time-invariant SST taken from the Real-Time Global SST (RTG-SST, http://polar.ncep.noaa.gov/sst/) analysis on 13 January 2005 00Z, and (2) *one-way coupled run*, WRF-only simulation with a low resolution SST linearly interpolated every 3 h from daily RTG-SST data from 13 to 31 January 2005. We note that employing a static SST condition as in the uncoupled run represents a standard method for handling SST in short (days to weeks) atmospheric model forecasts. Time series comparisons (not shown) show that surface winds, SLP, and surface air temperature are well-resolved by the atmospheric model regardless of which SST bottom boundary condition is used, though two-way coupling improves SST errors by up to 1.1 °C during the fast-moving ETC. We would anticipate that the effect of coupling would be significant in a case where the SST change is greater, especially if the low-pressure center was tracking over the area where the fastest SST changes were occurring. Future studies are therefore much needed. Nelson and He (2012), through a more detailed theoretical analysis, show that synoptic surface wind convergence is inversely proportional to the Laplacian of ocean surface temperature. Such two-way air–sea interactions can be derived from rather simple, linear Ekman and geostrophic dynamics in the MABL model of Lindzen and Sumant (1987). Only the two-way coupled model can represent a strong coupling of the upper ocean and the atmospheric boundary layer that exists for winter storms, particularly the cold air regime and upper ocean cooling directly following the storm, and thus arrive at the best agreement with a theoretical basis on the relationship between surface wind convergence and Laplacian of SST (Nelson and He 2012). A two-way coupled model proves most critical during the cold air outbreak in order to capture the changes in the wind field that are driven by the ocean cooling after the storm passes. We conclude that in order to improve ETC predictions and regional coastal wind and wind energy potential assessment in general, dynamic air–sea interactions altering momentum and heat fluxes have to be accurately accounted for in a coupled atmosphere–ocean modeling framework.

Acknowledgments We are grateful to the funding support provided by USGS Coastal Process project, NSF grant OCE-0927470, and ONR grant N00014-06-1-0739, and NASA grants NNX10AU06G, NNX12AP84G, and NNX13AD80G. Dr. Z. Yao's help in setting up the ocean model and J. Warrilow's editorial assistance are appreciated.

References

Bane JM, Osgood KE (1989) Wintertime air-sea interaction processes across the Gulf stream. J Geophys Res 94:10755–10772

Booij N, Ris RC, Holthuijsen LH (1999) A third-generation wave model for coastal regions. Part I: Model description and validation. J Geophys Res 104:7649–7666

Colucci SJ (1976) Winter cyclone frequencies over the eastern United States and adjacent western Atlantic, 1964–1973. Bull Am Meteorol Soc 57:548–553

DeGaetano AT (2008) Predictability of seasonal east coast winter storm surge impacts with application to New York's Long Island. Meteor Appl 15:231–242

Dirks RA, Kuettner JP, Moore JA (1988) Genesis of atlantic lows experiment (GALE): an overview. Bull Am Meteorol Soc 69:148–160

Fairall CW, Bradley EF, Rogers DP, Edson JB, Young GS (1996) Bulk parameterization of air-sea fluxes for tropical ocean-global atmosphere coupled-ocean atmosphere response experiment. J Geophys Res 101:3747–3764

Flather RA (1976) A tidal model of the north-west European continental shelf. Mem Soc R Sci Liege 6:141–164

Hirsch ME, DeGaetano AT, Colucci SJ (2001) An east coast winter cyclone climatology. J Clim 14:882–899

Jones PW (1998) A user's guide for SCRIP: a spherical coordinate remapping and interpolation package. Los Alamos National Laboratory. WWW page: http://climate.lanl.gov/Software/SCRIP/

Kundu PK (1976) An analysis of inertial oscillations observed near the Oregon coast. J Phys Oceanogr 6:879–893

Larson J, Jacob R, Ong E (2005) The model coupling toolkit: a new FORTRAN90 toolkit for building multiphysics parallel coupled models. Int J High Perform C 19:277–292

Lindzen RS, Sumant N (1987) On the role of sea surface temperature gradients in forcing low-level winds and convergence in the tropics. J Atmos Sci 44:2418–2436

Marchesiello P, McWilliams JC, Shchepetkin A (2001) Open boundary conditions for long-term integration of regional ocean models. Ocean Modell 3:1–20

Mellor LG, Yamada T (1982) Development of a turbulence closure model for geophysical fluid problems. Geophys Space Phys 20: 851–875

Nelson JS, He R (2012) Effect of the Gulf Stream on winter extratropical cyclone outbreaks. Atmosph Sci Lett 13:311–316. doi:10.1002/asl.400

Olabarrieta M, Warner JC, Armstrong B, Zambon JB, He R (2012) Ocean–atmosphere dynamics during Hurricane Ida and Nor'Ida: an application of the coupled ocean–atmosphere-wave-sediment transport (COAWST) modeling system. Ocean Modell 43:112–137

Reddy NC, Raman S (1994) Observations of a mesoscale circulation over the Gulf Stream region. Global Atmos Ocean Syst 2:21–39

Sanders F, Gyakum JR (1980) Synoptic-dynamic climatology of the "bomb". Mon Weather Rev 108:1589–1606

Shchepetkin AF, McWilliams JC (2005) The regional ocean modeling system: a split-explicit, free-surface, topography-following coordinates ocean model. Ocean Modell 9:347–404

Skamarock WC, Klemp JB, Dudhia J, Gill DO, Barker DM, Duda MG, Huang X-Y, Wang W, Powers JG (2008) A description of the Advanced Research WRF Version 3. Technical note. National Center for Atmospheric Research, TN-475+STR. WWW page: http://www.mmm.ucar.edu/wrf/users/docs/arw_v3.pdf

Small RJ, deSzoeke SP, Xie SP, O'Neill L, Seo H, Song Q, Cornillon P, Spall M, Minobe S (2008) Air-sea interactions over ocean fronts and eddies. Dyn Atmos Oceans 45:274–319

Warner JC, Sherwood CR, Signell RP, Harris CK, Arango HG (2008) Development of a three-dimensional, regional, coupled wave, current, and sediment-transport model. Comput Geosci 34:1284–1306. doi:10.1016/j.cageo.2008.02.012

Warner JC, Armstrong B, He R, Zambon JB (2010) Development of a coupled-ocean–atmosphere-wave-sediment-transport (COAWST) modeling system. Ocean Modell 35:230–244. doi:10.1016/j.ocemod.2010.07.010

Wayland RJ, Raman S (1994) Structure of the marine atmospheric boundary layer during two cold air outbreaks of varying intensities: GALE 86. Bound-Layer Meteor 71:43–66

Xue H, Bane JM, Goodman LM (1995) Modification of the Gulf stream through strong air-sea interactions in winter: observations and numerical simulations. J Phys Oceanogr 25:533–557

Zishka KM, Smith PJ (1980) The climatology of cyclones and anticyclones over North America and surrounding ocean environs for January and July, 1950–77. Mon Weather Rev 108:387–401